Pressure-Induced New Topological Weyl Semimetal Phase in TaAs

Yonghui Zhou,[1,2] Pengchao Lu,[3] Yongping Du,[3] Xiangde Zhu,[1] Ganghua Zhang,[4] Ranran Zhang,[1] Dexi Shao,[3] Xuliang Chen,[1,2] Xuefei Wang,[2] Mingliang Tian,[1,5] Jian Sun,[3,5,*] Xiangang Wan,[3,5,†] Zhaorong Yang,[1,2,5,‡] Wenge Yang,[4,6,§] Yuheng Zhang,[1,5] and Dingyu Xing[3,5]

[1]*High Magnetic Field Laboratory, Chinese Academy of Sciences, Hefei 230031, China*
[2]*Key Laboratory of Materials Physics, Institute of Solid State Physics, Chinese Academy of Sciences, Hefei 230031, China*
[3]*National Laboratory of Solid State Microstructures, School of Physics, Nanjing University, Nanjing 210093, China*
[4]*Center for High Pressure Science and Technology Advanced Research (HPSTAR), Shanghai 201203, China*
[5]*Collaborative Innovation Center of Advanced Microstructures, Nanjing University, Nanjing 210093, China*
[6]*High Pressure Synergetic Consortium (HPSynC), Geophysical Laboratory, Carnegie Institution of Washington, 9700S Cass Avenue, Argonne, Illinois 60439, USA*

(Received 11 March 2016; revised manuscript received 12 August 2016; published 28 September 2016)

We report a new pressure-induced phase in TaAs with different Weyl fermions than the ambient structure with the aid of theoretical calculations, experimental transport and synchrotron structure investigations up to 53 GPa. We show that TaAs transforms from an ambient $I4_1md$ phase (t-TaAs) to a high-pressure hexagonal P-6m2 (h-TaAs) phase at 14 GPa, along with changes of the electronic state from containing 24 Weyl nodes distributed at two energy levels to possessing 12 Weyl nodes at an isoenergy level, which substantially reduces the interference between the surface and bulk states. The new pressure-induced phase can be reserved upon releasing pressure to ambient condition, which allows one to study the exotic behavior of a single set of Weyl fermions, such as the interplay between surface states and other properties.

DOI: 10.1103/PhysRevLett.117.146402

A Weyl semimetal (WSM) is considered a three-dimensional analog of graphene in terms of its electronic dispersion. One of the most striking characteristics of a WSM is the topological surface state with Fermi arcs. This was first proposed in pyrochlore iridates in 2011 [1] and extended to several other systems by different groups [2–5]. With the Weyl nodes behaving like Weyl fermions [1,2], WSM possess novel transport properties stemming from the chiral anomaly [6–8]. Weyl nodes appear in pairs of opposite chirality due to the "No-go theorem." Recently, the noncentrosymmetric NbAs-type transition-metal monoarsenides, i.e., TaAs, TaP, NbAs, and NbP, have been predicted to be WSMs. Furthermore, all these four NbAs-type WSMs have twelve pairs of Weyl nodes in their 3D Brillouin zones [9,10], and are completely stoichiometric and nonmagnetic, which provides a good platform for the novel property study in the topological WSMs. Soon after, many exotic properties associated with WSM have been observed, such as Weyl nodes, Fermi arcs [11–14] and the negative longitudinal magnetoresistance (MR) [15–17] due to the chiral anomaly [18–22]. These results demonstrate that the TaAs family is a promising system that hosts topological properties, which might have potential applications in electronics, optoelectronics, and quantum computing [23].

The 24 Weyl nodes in TaAs can be classified to two types, which locate at two different energy levels with considerable trivial Fermi pockets. The contribution from these trivial states complicates the analysis of topological surface states and novel transport behaviors [10,11]. Thus, it would be interesting to find ways to reduce the number of Weyl nodes, degenerate them close to the Fermi level, and, consequently, minimize the interference from the trivial states. High pressure has been considered as an effective and clean way to tune lattice as well as electronic states, especially in quantum states [24–26]; thus, it would be important to investigate the pressure effect on the Weyl nodes and size of the topological trivial Fermi surfaces.

In this Letter, we report a joint study of the evolution of the electronic and structural properties of single-crystal TaAs under high pressure, from both *ab initio* calculations and experimental measurements, including electrical resistance measurements and synchrotron x-ray diffraction (XRD) experiments. Our theoretical predictions and experimental results show that the Weyl nodes in the $I4_1md$ (t-TaAs) structure remain stable upon compression up to 14 GPa and a new P-6m2 (h-TaAs) phase with only one type of Weyl nodes emerges above 14 GPa. Upon decompression, this high-pressure h-TaAs phase can be kept to ambient pressure, which may allow one to study this new Weyl semimetal further at ambient conditions.

Theoretical calculations and experimental details are presented in the Supplemental Material [27]. The ambient TaAs crystallizes in a body-centered tetragonal NbAs-type structure with the noncentro-symmetric space group $I4_1md$ (D_{4v}^{11}, No. 109) [37], as shown in Fig. 1(c). The absence of a horizontal mirror plane in the unit cell breaks the inversion symmetry. It is known that the ambient t-TaAs structure has two kind of Weyl nodes. One type locates in the $k_z = 0$

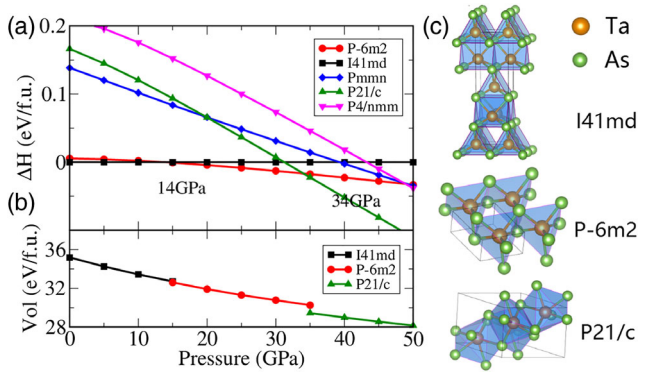

FIG. 1. (a) Calculated enthalpy relative to that of the $I4_1md$ (t-TaAs) phase at pressure up to 50 GPa. (b) Unit cell volume vs pressure. (c) Crystal structures of ambient phase (t-TaAs) and the two best candidates of high-pressure phases [P-6m2 (h-TaAs) and $P2_1/c$ (m-TaAs)]. Brown and green balls represent the Ta atom and As atom, respectively.

plane (W1), and the other is off this plane (W2) [10,11]. These two sets of Weyl nodes have an energy difference of about 14 meV at ambient pressure [11]. Pressure is utilized to tune these energy levels. As shown in the Supplemental Material, Table I, the Weyl nodes in the t-TaAs phase are quite robust upon compression. We also calculated the band structures of the t-TaAs phase at different pressures (see Supplemental Material [27], Fig. S1). The overall shape of the band structure near the Fermi level does not change much upon compression. With increasing pressure, the electron pockets become smaller while the hole pockets become larger, suggesting a multicarrier system.

To check the energy favorite phases at higher pressure, we utilized crystal structure prediction techniques with the density functional theory (DFT) to calculate the enthalpy of all candidates of TaAs at each pressure. The enthalpy-pressure (ΔH-P) plots against the t-TaAs structure are shown in Fig. 1(a) at pressures up to 50 GPa. The ambient structure of TaAs is found to be t-TaAs, which is consistent with the experimental observations [37]. From 14 to 34 GPa, the calculation predicts a h-TaAs structure has lower enthalpy than that of the t-TaAs structure. These two structures have the same type $TaAs_6$ polyhedron and a triangular prism with almost the same triangle side length and height, but different stacking sequences of the triangular prisms as shown in Fig. 1(c). The t-TaAs structure is constructed with an AB sequence along the c axis, while the h-TaAs structure has a uniform AA stacking. When the pressure reaches beyond 34 GPa, a $P2_1/c$ (m-TaAs) structure becomes the most energy favorite one. The crystal structure of the m-TaAs phase is nonmagnetic with inversion symmetry; thus, Weyl nodes are no longer preserved. As shown in the Supplemental Material [27], Fig. S2, the h-TaAs and m-TaAs phases are found to be dynamically stable at high and ambient pressure.

The band structure and Fermi surface of the high-pressure h-TaAs phase are calculated as shown in Fig. 2. The bands are overlapping near the A point which behaves like a metallic phase, while the spin-orbit coupling opens a gap of around 160 meV for the crossing point near the K point. On the other hand, as shown in the Supplemental Material [27], Fig. S3(a) without SOC, there is a band inversion around K point. The hybridization between two bands belonging to two different irreducible representations is strictly forbidden, which results in the protected band crossing along the K-Γ and K-M lines and a gapless nodal ring around the K point in the Γ-K-M plane.

The intriguing electronic structures of h-TaAs encourage us to investigate its topological properties. Interestingly, our calculations show that this noncentro-symmetric structure is also a Weyl semimetal. This phase has fewer Weyl nodes (12 in the 1st Brillouin zone) as shown in Fig. 2(c). More interestingly, all 12 Weyl nodes belong to the same type and are related to each other by symmetry; consequently, they have the same energy. The Weyl nodes obtained from scanning in the $k_z = 0.027$ plane (parallel to Γ-K-M) and the Γ-K-A plane are shown in Figs. 2(d) and 2(e), respectively. As presented in the Supplemental Material [27], Table II, the position of these Weyl nodes in the h-TaAs structure stays almost unchanged, while the pressure has considerable effect on the position of Weyl nodes in the t-TaAs phase.

To further investigate the topological properties of TaAs in the h-TaAs phase, we calculate the (100) surface state. The bulk Brillouin zone and the projected (100) surface Brillouin zone are shown in Fig. 3(b). One of the fundamental characteristics of the WSM is the existence of Fermi arcs [1]. There is a simple and effective way to verify the existence of a nontrivial surface state [12–14]. We choose a generic closed loop in the 2D surface Brillouin zone, and count the number of Fermi surface crossings through this

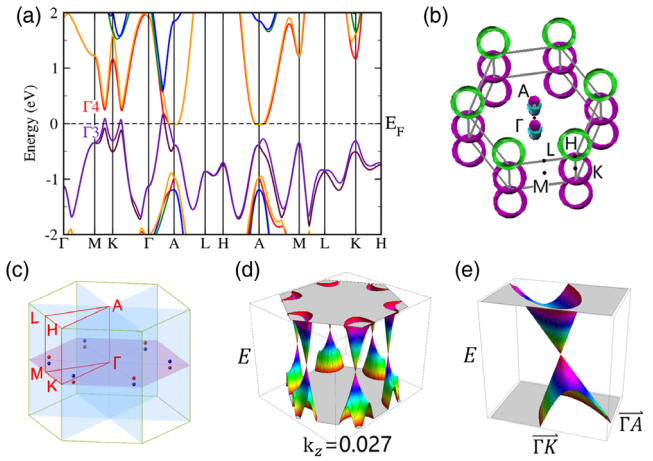

FIG. 2. Calculated electronic band structures of TaAs in the h-TaAs phase at 25 GPa. (a) Electronic band structures with spin-orbit coupling. (b) Calculated Fermi surfaces of the h-TaAs phase. (c) The Weyl nodes distribution in the first Brillouin zone. The Weyl nodes obtained from scanning in the $k_z = 0.027$ plane (parallel to Γ-K-M) (d) and Γ-K-A plane (e), respectively.

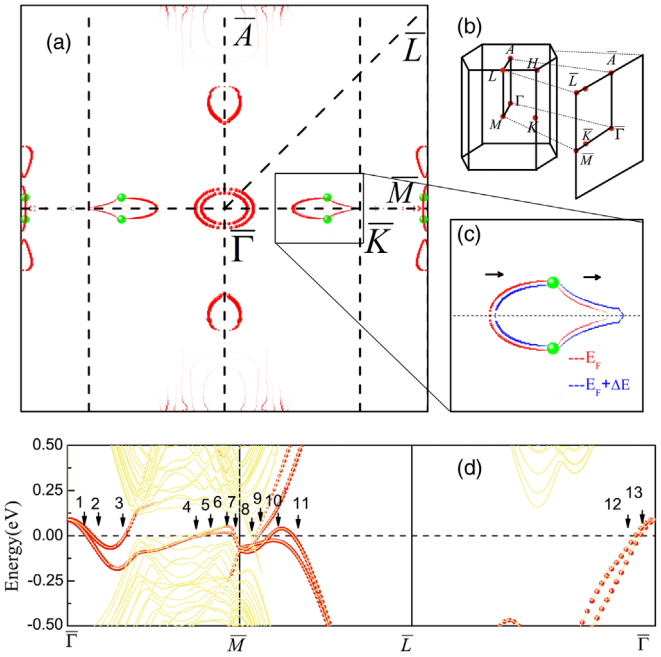

FIG. 3. Topological properties of TaAs in the *h*-TaAs phase. (a) The surface state of As termination of TaAs in the *h*-TaAs phase. Green dots are the bulk Weyl nodes projected to the 2D surface Brillouin zone. (b) The 3D Brillouin zone and the projected 2D surface Brillouin zone. (c) Evolution of the constant energy contour of two Fermi arcs. It can be seen that the two arcs move to the same direction as the energy shifts. (d) The band structure of the (100) surface along the closed loop ($\bar{\Gamma}$-$\bar{M}$-$\bar{L}$-$\bar{\Gamma}$). The red dots are the surface electronic structure which projected to As termination.

loop. The Fermi surface would cross the closed loop an even number of times unless it is unclosed (Fermi arc). As shown in Fig. 3(a), we choose $\bar{\Gamma}$-$\bar{M}$-$\bar{L}$-$\bar{\Gamma}$ as a closed loop to count the Fermi surface crossing. There are two Weyl nodes projected to the same point on the surface near $\bar{K}$ (position 1, *P*1) and one Weyl node projected on the surface near $\bar{M}$ (position 2, *P*2). Hence, three Weyl points are enclosed in this loop. The number of Fermi surface crossing is expected to be odd. The surface band structure along $\bar{\Gamma}$-$\bar{M}$-$\bar{L}$-$\bar{\Gamma}$ is illustrated in Fig. 3(d), the red dots are the surface states which are projected to the As termination. We can count that the number of crossings is 13. This proves that the nontrivial surface states, Fermi arcs, exist on the (100) surface of TaAs.

The Fermi arcs can also be clarified by studying the evolution of the constant energy contours as a function of energy [11]. Two Fermi arcs move toward the same direction as one varies energy, while the trivial closed surface state would move to the opposite direction [11]. Figure 3(c) shows that the two Fermi surfaces around the *P*1 move to the same direction as the energy is increased by 20 meV. As a result, these two surface states become Fermi arcs.

To confirm the possible phase transition from the theoretical prediction, the TaAs sample was subjected to *in situ* high-pressure synchrotron XRD study. The angle-dispersive XRD experiments were conducted with diamond anvil cells up to 53.11 GPa. The powder diffraction profiles during compression and decompression are shown in Supplemental Fig. S4 [27]. The diffraction data clearly confirm the phase transition from the *t*-TaAs phase to the *h*-TaAs phase at 14 GPa. The evolutions of lattice parameter *a*, *c*, and volume V/Z (unit cell volume per TaAs formula) up to 53.11 GPa are plotted in Figs. 4(a)–4(c). It is clear that the long-ordered structure along the *c* axis in *t*-TaAs collapses to a similar lattice constant of hexagonal phase *h*-TaAs. We noticed the peak broadening of 10.5 degrees at 10.41 GPa, which indicates the settle in of the high-pressure phase. But the percentage of the high-pressure phase is too low to fit reliable lattice parameters. So we call the transition pressure 14.40 GPa thereafter. The detail GSAS Rietveld refinements at 0.22 (pure *t*-TaAs phase), 16.15 (mixture of *t*-TaAs and *h*-TaAs), and 53.11 GPa (pure high-pressure *h*-TaAs phase) show good fittings of the predicted structures (see Fig. 4 and the Supplemental Material, Fig. S5). Meanwhile, the structure of 0.74 GPa data obtained from the lowest decompression pressure shown in Fig. 4(f) can be refined by the *h*-TaAs structure, suggesting that the high-pressure hexagonal phase is reserved. Although the prediction of the transition pressure from *t*-TaAs to *h*-TaAs at 14 GPa is almost exactly the same as XRD observations, up to 53.11 GPa we did not observe the second high-pressure phase transition from *h*-TaAs to *m*-TaAs predicted around 37 GPa. The *t*-TaAs and *h*-TaAs structures have the same $TaAs_6$ polyhedron but

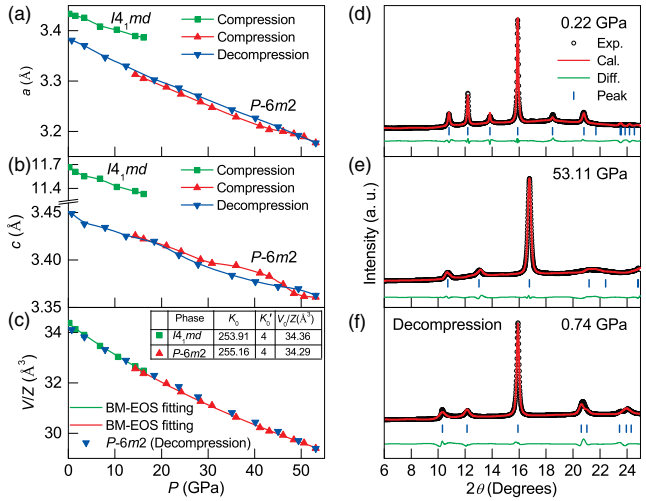

FIG. 4. High-pressure synchrotron XRD patterns of TaAs. Structural analysis reveals the irreversible phase transition $I4_1md$ (*t*-TaAs) to *P*-6*m*2 (*h*-TaAs) in TaAs upon decompression. (a) Lattice constant *a*, (b) lattice constant *c*, and (c) unit cell volume vs pressure. Representative Rietveld refinements at (d) 0.22 and (e) 53.11 GPa upon compression, respectively. (f) The pattern at 0.74 GPa upon decompression can be refined by the *h*-TaAs structure, suggesting that the high-pressure hexagonal phase is reserved.

with different stacking sequences. Therefore, their enthalpies are very close to each other. In fact, the high-pressure synchrotron XRD experiments suggest that these two phases may coexist at pressures above the predicted critical pressure. In contrast, the *m*-TaAs phase consists of $TaAs_7$ polyhedron. The phase transition from the *h*-TaAs to *m*-TaAs needs large rearrangement of atoms, and breaking or reforming of chemical bonds, which can bring a huge transition barrier and may hinder the transition from the *h*-TaAs to *m*-TaAs. However, with both inversion symmetry and time reverse symmetry, the *m*-TaAs phase cannot be a Weyl semimetal, which is out of our current research interest.

In order to examine the effect of structural phase transition on the transport properties, we further performed high-pressure resistance measurements. At ambient pressure TaAs exhibits a metalliclike behavior down to 2 K (see Supplemental Fig. S8). After applying external pressure of 1.1 GPa, the temperature dependence of resistance exhibits a semiconductinglike behavior ($d\rho/dT < 0$) over the entire measured temperature range, as shown in Fig. 5(a). The pressure-induced metal-semiconducting transition intuitively resembles the case of the magnetic field effect on the resistance [see Fig. S8(b)]. Normally pressure enhances the band overlapping, the pressure-induced metal-semiconducting transition is indeed very unusual and not yet well understood. A similar phenomenon has been reported in other Dirac materials, such as Cd_3As_2 [38,39], Bi_2Se_3 [40] and Sr-doped Bi_2Se_3 [41]. However, a common character in the Dirac materials is the high mobility of charge carriers. For example, the mobility of TaAs is 1.8×10^5 $cm^2\,V^{-1}\,s^{-1}$ at 10 K, which drops by almost 2 orders of magnitude upon warming to room temperature [16]. One possible reason for the semiconducting behavior under pressure is the suppression of mobility while carrier density changes little, similar to the case of Bi_2Se_3 [40]. This is because the mobility is very sensitive to the defects and stress induced by the pressure. From 1.1 to 10.0 GPa, the $R(T)$ curve keeps the semiconductinglike behavior. Nevertheless, this is not the case of isostructural NbAs, which remains a metallic behavior up to 20 GPa [42]. The resistance at 300 K increases monotonically, while the resistance at 1.8 K first increases with pressure then decreases above 5.0 GPa [see Fig. 5(c)]. Accordingly, when the pressure is increased to 14.0 GPa, a semiconductinglike to metalliclike transition emerges upon cooling, showing a resistance hump at $T_{M-I} \sim 140$ K. The hump in TaAs is very similar to the conduction of Dirac semimetal $ZrTe_5$ single crystal, where the resistivity anomaly could be attributed to the temperature-induced Lifshitz transition as recently revealed by angle-resolved photoemission spectroscopy (ARPES) measurements [43]. With further increasing pressure, the T_{M-I} shifts to higher temperatures.

Since TaAs possesses large MR in analogy to WTe_2 [44], which has been predicted very recently to be a new type of

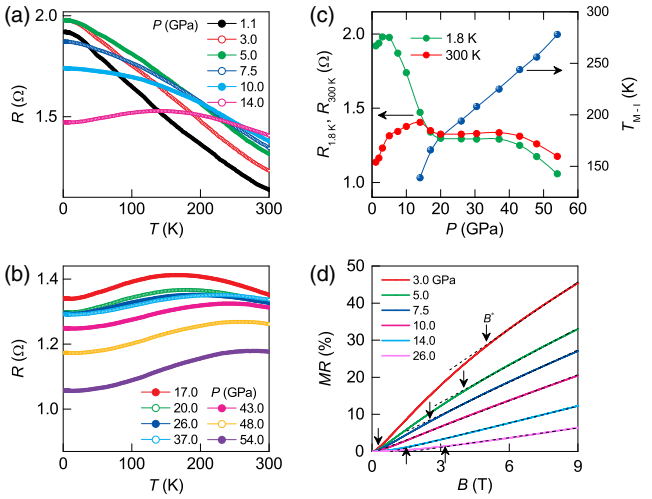

FIG. 5. Temperature dependences of resistance of a TaAs single crystal at various pressures. (a),(b) Sample resistance profiles vs temperature under high pressure. (c) The semiconductor-metal transition temperature T_{M-I} and specific resistance as a function of applied pressure at 1.8 and 300 K, respectively. The T_{M-I} is defined as the hump on the resistance curve. (d) Isothermal magnetoresistance at 4.5 K under representative pressures. The dashed lines denote the linear behavior. The arrows represent the characteristic magnetic field B^*, below which the magnetoresistance deviates significantly from linearity.

WSM [45], we investigated the MR at 4.5 K under different pressures. As shown in Fig. 5(d), no Shubnikov–de Haas oscillations up to 9 T can be observed after applying external pressure, which could be attributed to the suppression of mobility of the charge carrier as discussed above. On the other hand, the MR is dramatically suppressed by pressure, which is similar to the case of pressurized WTe_2 [46,47]. In WTe_2, the suppression of MR is accompanied by the emergence of superconductivity [47,48]. However, in our case, no hint of a resistance drop appears even down to 1.8 K until 54.0 GPa. Nevertheless, note that the MR curve at 10.0 GPa displays a linear behavior in a broad field region. As shown in Fig. 5(d), the characteristic field B^*, above which the linear MR is observed, first shifts monotonically to lower fields with increasing pressure from 3.0 GPa, then turns back for pressures above 10.0 GPa. Similar curvature changes in the MR curve have been observed in pressurized Ag_2Te due to pressure-induced crossover from *p*-type to *n*-type conductivity [49]. Combining with the fact that a semiconducting-like to metalliclike transition emerges upon cooling above 10.0 GPa, it can be deduced that this pressure is close to the critical pressure corresponding to the structural and topological phase transition as revealed by theoretical prediction and XRD results. The critical pressure close to 10.0 GPa is also revealed in Fig. 5(c), where the room-temperature resistance displays a maximum at 14.0 GPa, levels off in the pressure region from 20.0 to 37.0 GPa, and then drops slightly afterwards.

In summary, by combining theoretical and experimental investigations, we confirmed a new Weyl semimetal phase with a hexagonal lattice induced by pressure in TaAs at 14 GPa. Comparing to 24 Weyl nodes distributed at two different energy levels in the ambient tetragonal phase, the high-pressure hexagonal phase is predicted to be a new topological semimetal with only 12 Weyl nodes at the same energy level. Decompression XRD experiments confirmed that the hexagonal phase is metastable at ambient pressure once it is formed beyond 14 GPa, which provides an excellent platform to study the interplay between surface states and other exotic properties without the limitation of access due to high pressure environments. As this is the first report of pressure-induced isoenergetic Weyl fermions in TaAs, further investigations on the novel surface electronic states and other possible exotic properties are desired.

This research was financially supported by projects from the MOST of China (Grants No. 2016YFA0300404, No. 2015CB921202, and No. 2016YFA0401804), the NSFC (Grants No. 51372112, No. 11525417, No. 11574133, No. U1530402, No. 11574323, and No. U1332143), NSF Jiangsu province (No. BK20150012), and the Fundamental Research Funds for the Central Universities and Special Program for Applied Research on Super Computation of NSFC-Guangdong Joint Fund (2nd phase). Part of the calculations were performed on the supercomputer in the High Performance Computing Center of Nanjing University. W. Y. acknowledges the financial support from the DOE-BES X-ray Scattering Core Program under Grant No. DE-FG02-99ER45775. The XRD measurements were performed at the BL15U1 beam line, Shanghai Synchrotron Radiation Facility (SSRF) in China. The authors would like to thank Dr. Ke Yang and Dr. Shuai Yan for beam line technical support.

Y. Z, P. L., Y. D., and X. Z. contributed equally to this work.

Note added.—Recently, the understanding of the electronic structures of this type of structure reached a new level. We realize Weyl fermion and massless triply degenerate nodal points [50] coexist in our *h*-TaAs, similar to ZrTe [51]. Meanwhile, a prediction for similar structures with a different method is reported [52]. Structures proposed by another work [53] seem to not fit to our experimental XRD data.

*jiansun@nju.edu.cn
†xgwan@nju.edu.cn
‡zryang@issp.ac.cn
§yangwg@hpstar.ac.cn

[1] X. Wan, A. M. Turner, A. Vishwanath, and S. Y. Savrasov, Phys. Rev. B **83**, 205101 (2011).
[2] G. Xu, H. Weng, Z. Wang, X. Dai, and Z. Fang, Phys. Rev. Lett. **107**, 186806 (2011).
[3] P. Hosur, Phys. Rev. B **86**, 195102 (2012).
[4] T. Ojanen, Phys. Rev. B **87**, 245112 (2013).
[5] A. C. Potter, I. Kimchi, and A. Vishwanath, Nat. Commun. **5**, 5161 (2014).
[6] A. A. Zyuzin and A. A. Burkov, Phys. Rev. B **86**, 115133 (2012).
[7] Z. Wang and S.-C. Zhang, Phys. Rev. B **87**, 161107(R) (2013).
[8] S. A. Parameswaran, T. Grover, D. A. Abanin, D. A. Pesin, and A. Vishwanath, Phys. Rev. X **4**, 031035 (2014).
[9] S.-M. Huang *et al.*, Nat. Commun. **6**, 7373 (2015).
[10] H. Weng, C. Fang, Z. Fang, B. A. Bernevig, and X. Dai, Phys. Rev. X **5**, 011029 (2015).
[11] S.-Y. Xu *et al.*, Science **349**, 613 (2015).
[12] B. Q. Lv *et al.*, Phys. Rev. X **5**, 031013 (2015).
[13] L. X. Yang *et al.*, Nat. Phys. **11**, 728 (2015).
[14] D. F. Xu, Y.-P. Du, Z. Wang, Y.-P. Li, X.-H. Niu, Q. Yao, D. Pavel, Z.-A. Xu, X.-G. Wan, and D.-L. Feng, Chin. Phys. Lett. **32**, 107101 (2015).
[15] C. Zhang *et al.*, arXiv:1502.00251.
[16] X. Huang *et al.*, Phys. Rev. X **5**, 031023 (2015).
[17] C. Shekhar *et al.*, Nat. Commun. **7**, 11615 (2016).
[18] H. B. Nielsen and M. Ninomiya, Phys. Lett. B **130**, 389 (1983).
[19] V. Aji, Phys. Rev. B **85**, 241101(R) (2012).
[20] D. T. Son and B. Z. Spivak, Phys. Rev. B **88**, 104412 (2013).
[21] H.-J. Kim, K. S. Kim, J. F. Wang, M. Sasaki, N. Satoh, A. Ohnishi, M. Kitaura, M. Yang, and L. Li, Phys. Rev. Lett. **111**, 246603 (2013).
[22] P. Hosur and X. Qi, C.R. Phys. **14**, 857 (2013).
[23] D. Ciudad, Nat. Mater. **14**, 863 (2015).
[24] J. L. Zhang *et al.*, Proc. Natl. Acad. Sci. U.S.A. **108**, 24 (2011).
[25] C. Zhang, L. Sun, Z. Chen, X. Zhou, Q. Wu, W. Yi, J. Guo, X. Dong, and Z. Zhao, Phys. Rev. B **83**, 140504(R) (2011).
[26] K. Kirshenbaum, P. S. Syers, A. P. Hope, N. P. Butch, J. R. Jeffries, S. T. Weir, J. J. Hamlin, M. B. Maple, Y. K. Vohra, and J. Paglione, Phys. Rev. Lett. **111**, 087001 (2013).
[27] See Supplemental Material at http://link.aps.org/supplemental/10.1103/PhysRevLett.117.146402 for the band calculation and experimental details and the supporting results, which includes Refs. [28–36].
[28] G. Kresse and J. Furthmller, Comput. Mater. Sci. **6**, 15 (1996).
[29] J. P. Perdew, K. Burke, and M. Ernzerhof, Phys. Rev. Lett. **77**, 3865 (1996).
[30] A. Togo, F. Oba, and I. Tanaka, Phys. Rev. B **78**, 134106 (2008).
[31] P. Blaha *et al.*, *WIEN2k, An Augmented Plane Wave Plus Local Orbitals Program for Calculating Crystal Properties* (TU Vienna, Vienna, 2001).
[32] J. Kuneš, P. Novak, R. Schmid, P. Blaha, and K. Schwarz, Phys. Rev. B **64**, 153102 (2001).
[33] A. P. Hammersley, S. O. Svensson, M. Hanfland, A. N. Fitch, and D. Hausermann, High Press. Res. **14**, 235 (1996).
[34] A. C. Larsen and R. B. Von Dreele, Los Alamos National Laboratory, Report LAUR 86-748, 2000.
[35] H. K. Mao, J. Xu, and P. M. Bell, J. Geophys. Res. **91**, 4673 (1986).
[36] C. Zhang *et al.*, arXiv:1503.02630.
[37] H. Boller and E. Parthé, Acta Crystallogr. **16**, 1095 (1963).
[38] S. Zhang *et al.*, Phys. Rev. B **91**, 165133 (2015).
[39] L. P. He *et al.*, arXiv:1502.02509.

[40] J. J. Hamlin, J. R. Jeffries, N. P. Butch, P. Syers, D. A. Zocco, S. T. Weir, Y. K. Vohra, J. Paglione, and M. B. Maple, J. Phys. Condens. Matter **24**, 035602 (2012).
[41] Y. Zhou, X. Chen, R. Zhang, J. Shao, X. Wang, C. An, Y. Zhou, C. Park, W. Tong, L. Pi, Z. Yang, C. Zhang, and Y. Zhang, Phys. Rev. B **93**, 144514 (2016).
[42] J. Zhang, F.-L. Liu, J.-K. Dong, Y. Xu, N.-N. Li, W.-G. Yang, and S.-Y. Li, Chin. Phys. Lett. **32**, 097102 (2015).
[43] Y. Zhang *et al.*, arXiv:1602.03576.
[44] M. N. Ali *et al.*, Nature (London) **514**, 205 (2014).
[45] A. A. Soluyanov, D. Gresch, Z. Wang, Q. S. Wu, M. Troyer, X. Dai, and B. Andrei Bernevig, Nature (London) **527**, 495 (2015).
[46] P. L. Cai, J. Hu, L. P. He, J. Pan, X. C. Hong, Z. Zhang, J. Zhang, J. Wei, Z. Q. Mao, and S. Y. Li, Phys. Rev. Lett. **115**, 057202 (2015).
[47] X.-C. Pan *et al.*, Nat. Commun. **6**, 7805 (2015).
[48] D. Kang *et al.*, Nat. Commun. **6**, 7804 (2015).
[49] M. Lee, T. F. Rosenbaum, M.-L. Saboungi, and H. S. Schnyders, Phys. Rev. Lett. **88**, 066602 (2002).
[50] H. Weng, C. Fang, Z. Fang, and X. Dai, Phys. Rev. B **93**, 241202(R) (2016).
[51] H. Weng *et al.*, arXiv:1605.05186.
[52] M. Lu, Y. Guo, M. Zhang, H. Liu, and J. S. Tse, Solid State Commun. **240**, 37 (2016).
[53] J. Buckeridge, D. Jevdokimovs, C. R. A. Catlow, and A. A. Sokol, Phys. Rev. B **93**, 125205 (2016).